

A GLOBAL PROBE OF COSMIC MAGNETIC FIELDS TO HIGH REDSHIFTS

P. P. KRONBERG^{1,2}, M. L. BERNET³, F. MINIATI³, S.J. LILLY³, M. B. SHORT¹, D. M. HIGDON¹
Astrophysical Journal, in press

ABSTRACT

Faraday rotation (RM) probes of magnetic fields in the universe are sensitive to cosmological and evolutionary effects as z increases beyond ~ 1 because of the scalings of electron density and magnetic fields, and the growth in the number of expected intersections with galaxy-scale intervenors, dN/dz . In this new global analysis of an unprecedented large sample of RM's of high latitude quasars extending out to $z \sim 3.7$ we find that the distribution of RM broadens with redshift in the 20 – 80 rad m⁻² range, despite the $(1+z)^{-2}$ wavelength dilution expected in the observed Faraday rotation. Our results indicate that the Universe becomes increasingly “Faraday-opaque” to sources beyond $z \sim 2$, that is, as z increases progressively fewer sources are found with a “small” RM in the observer’s frame. This is in contrast to sources at $z \lesssim 1$. They suggest that the environments of galaxies were significantly magnetized at high redshifts, with magnetic field strengths that were at least as strong within a few Gyr of the Big Bang as at the current epoch. We separately investigate a simple unevolving toy model in which the RM is produced by MgII absorber systems, and find that it can approximately reproduce the observed trend with redshift. An additional possibility is that the intrinsic RM associated with the radio sources was much higher in the past, and we show that this is not a trivial consequence of the higher radio luminosities of the high redshift sources.

Subject headings: galaxies: high redshift – quasars: general – cosmology: magnetic Fields — methods: data analysis

1. INTRODUCTION

The strengths of interstellar and intergalactic magnetic fields at earlier epochs have important implications for galaxy and structure evolution (e.g. Mestel & Paris 1984; Rees 1987), the propagation of ultra-high energy cosmic rays (Sigl, Miniati, & Enblin 2003, 2004; Armengaud, Sigl & Miniati, 2005; Dolag et al. 2005), and the feedback of magnetic energy into the intergalactic medium by stellar winds and early massive black holes (Kronberg et al. 2001).

Faraday rotation of distant polarized radio sources is one of the few available measurables to detect and probe extragalactic magnetic fields. For a cosmologically distant polarized source at redshift z_s it is defined, in units of rad/m², as:

$$RM(z_s) = \frac{\Delta\chi_0}{\Delta\lambda_0^2} = 8.1 \cdot 10^5 \int_0^{z_s} \frac{n_e(z) B_{\parallel}(z)}{(1+z)^2} \frac{dl}{dz} dz. \quad (1)$$

The RM describes the change in polarization angle $\Delta\chi_0$ with respect to a change in wavelength squared $\Delta\lambda_0^2$ due to the presence of a magnetized medium (the subscript 0 indicates observer’s frame). In Eq. (1) the free electron number density, n_e , is in cm⁻³, B_{\parallel} , in Gauss, is the line of sight component of the magnetic field and dl/dz , in parsecs, is the comoving path increment per unit redshift. In general the total RM of a given radio source will be a sum of several different components: (1) a “smooth” Galactic component, defined as SRM, that may be assumed to vary with l and b on angular scales that are larger than the typical inter-source separation. This also

includes any metagalactic and/or local universe RM contributions that might exist on large angular scales; (2) A component arising from intervening discrete clouds, e.g. galaxies, and/or a diffuse medium along the line of sight. The latter includes filaments of cosmological Large Scale Structure (LSS). The intervening galaxy system component should depend, statistically, only on the intergalactic path length traversed and not on direction. The third (3) is an “intrinsic” component from magnetised plasma associated with the distant radio source and its immediate environs, (RRM_{intr}), which may depend on source-intrinsic properties and which may also evolve cosmologically; Finally (4) there are measurement errors, which ideally should not depend on l , b , or z .

Detailed RM images of individual quasars between $z \sim 1$ and $z \sim 2$ with companion absorption line data have established clear examples of case (2) e.g. PKS 1229-021 (Kronberg, Perry & Zukowski 1992), and of case (3), e.g. 3C191 at $z_s = 1.95$, which contains intrinsic RM variations at $\sim z_s$ of order 2000 rad m⁻² (Kronberg, Perry & Zukowski 1990). These studies probed the intervening Faraday-active gas by analysing both optical absorption lines and Faraday rotation images. More recently, two-dimensional RM images from larger samples of resolved high- z quasar radio maps (Athreya et al. 1998, and Carilli et al. 1997), also show similarly high Faraday rotations at $2 \lesssim z \lesssim 4$, which these authors interpreted as indicating that the intrinsic RM dominates, i.e. case (3).

Redshift-dependence of the SRM-corrected RRM(z) (RRM = RM - SRM) could be due to one or both of (2) or (3) above, and in each case is subject to the $(1+z)^{-2}$

¹ Los Alamos National Laboratory, P.O. Box 1663, Los Alamos NM 87545 USA; kronberg@lanl.gov, mbshort@lanl.gov, dhigdon@lanl.gov

² Department of Physics, University of Toronto, 60 St. George, Toronto M5S 1A7, Canada; kronberg@physics.utoronto.ca

³ Physics Department, Wolfgang-Pauli-Strasse 16, ETH Zürich, CH-8093 Zürich, Switzerland; mbernet@phys.ethz.ch, fm@phys.ethz.ch, simon.lilly@phys.ethz.ch

watering-down effect in equation (1). Earlier attempts were made to detect a z -dependence of quasar RM's (Rees & Reinhardt 1972, Kronberg & Simard-Normandin 1976) using RM data on samples of extragalactic radio sources. All of these showed some evidence for an increase in the observed RM of quasars at $z \gtrsim 1$. With somewhat better RM data, and with optical absorption line data for some quasars, it was found that high column density optical and HI absorption at intervening redshifts correlated with higher levels of observed RM (e.g. Kronberg & Perry 1982, Kronberg, Perry & Zukowski 1992, Oren & Wolfe 1995). This allowed some first estimates of magnetic field strengths in distant intervening galaxy systems.

Welter et al.(1984) found a clear growth of the overall width (variance) of $|\text{RRM}|(z)$ in a 116-quasar RM sample, recently confirmed in a smaller sample by You et al. (2003). Welter et al. also developed mathematical frameworks for connecting RM correlations to components (2) and (3). They tentatively favored (2) over (3) at redshifts up to $z \sim 2$. A framework has also been developed by Kolatt (1998) for an RM-based probe of the primordial magnetic field spectrum, related to cases (2) and (3). More recently, optical galaxy and RM data were combined to undertake the first magnetic field probe of LSS filaments in the local universe (Xu, et al. 2006). Magnetic fields in the cosmic voids of LSS have not yet been detected.

This paper analyses an optimized subset of a new, much expanded sample of 900 extragalactic RRM's with measured redshifts up to $z \sim 3.7$. These also have improved determinations of the (smoothed) Galactic and local universe foreground SRM contribution. We focus on the overall *distribution* of RRM's as a function of redshift as a diagnostic of magnetic fields in high redshift systems, in particular the little-explored z - dependence of $|\text{RRM}|$ at $|\text{RRM}| \lesssim 100 \text{ rad m}^{-2}$. This is distinct from previous investigations, summarized above, of the overall width, or variance of the RRM distributions.

The rest of the paper is organized as follows. In Section 2 the RM dataset is briefly described and in Section 3 we discuss the selection and optimization of the RM sample, as well as tests for unwanted selection effects. The key evidence for a redshift dependence of the RRM distribution is presented in Section 4. We interpret the observed effects in Section 5. In general terms, an increase in the width of the RM distribution requires the presence of substantial amounts of magnetized plasma at high redshift. As one hypothesis, we construct a model in which the RM arises due to the presence of magnetized clouds traced by MgII absorption systems (5.1). In section 6 we discuss the complexities of detecting an all-pervading, intergalactic magnetic field in the presence of other extragalactic RM contributions. Our conclusions are summarized in Section 7. Throughout the paper we assume a concordance cosmology with $H_0 = 70 \text{ km s}^{-1}\text{Mpc}^{-1}$, $\Omega_m = 0.25$, $\Omega_\Lambda = 0.75$.

2. THE DATASET

The expanded RM data include new linear polarization measurements by one of us (PPK), which favored quasars at larger redshifts, plus additional data from the literature. Our new sample of 901 quasars and radio galaxies is sufficiently large that we are able to choose an optimized

subset (by Galactic l, b location) of 268 objects distributed up to $z \sim 3.7$. This subset exceeds the previous all-sky 116 quasar sample of Welter et al. (1984) by a factor of 2.3. In addition, the average quality of RM measurement is improved, as is also the Galactic foreground correction, which used a new expanded sample of 1566 extragalactic radio source RM's, mostly at $|b| > 5^\circ$.

Accurate subtraction of the foreground Galactic SRM is important for obtaining the purest possible isolation of the extragalactic RRM. The SRM was estimated using a Bayesian, Gaussian process formulation applied to the larger all-sky sample of 1566 extra- galactic radio source RMs (Short, Higdon and Kronberg, 2007a,b) which gives an SRM estimate for any (l, b) location.

In that paper, a fairly general Gaussian process (GP) model for the surface of the unit sphere \mathcal{S} with great circle distance metric $d(\mathbf{s}_1, \mathbf{s}_2)$ is derived by taking a collection of uniform, regularly spaced knot locations $\mathbf{w}_1, \dots, \mathbf{w}_J$, and assigning to each of these locations a knot value x_1, \dots, x_J which are assumed to have iid $N(0, [J\lambda_x]^{-1})$ distributions, where iid denotes ‘‘independent and identically distributed.’’ Convolution of these knot values with a simple smoothing kernel $k(\cdot)$ then results in the GP model

$$u(\mathbf{s}) = \sum_{j=1}^J x_j k(d(\mathbf{s}, \mathbf{w}_j)), \quad \mathbf{s} \in \mathcal{S}. \quad (2)$$

Figure 1 shows an example where \mathcal{S} is the unit circle. As $J \rightarrow \infty$, the process $u(\mathbf{s})$ quickly converges to a stationary GP.

The convolution kernel $k(\cdot)$ is taken to be a normal density whose width is to be estimated. A recursive tessellation algorithm is used to distribute $J = 2562$ knots over the unit sphere, giving a neighboring knot-to-knot distance of approximately $2\pi/80$. The spatial SRM field $u(\mathbf{s})$ is given by (2) which requires that the knot values x_j and the kernel width be estimated from the radio source RMs. The $N = 1566$ observations taken at locations $\mathbf{s}_1, \dots, \mathbf{s}_N$ are modeled as

$$\mathbf{Y}(\mathbf{s}_i) = u(\mathbf{s}_i) + \epsilon_i, \quad i = 1, \dots, N$$

where the errors are independent with $N(0, [\omega_i \lambda_\epsilon]^{-1})$ distributions. The ω_i 's, which modify the error precision, account for the possibility that certain observations have been altered by individual source RM anomalies, inter-veners, very small scale local effects of the Milky Way, etc. When $\omega_i < 1$, the observation has been altered and is downweighted for the purpose of estimating the SRM field; when $\omega_i = 1$, the observation is assumed to be free of any of these altering effects.

From the analysis of Short et al. (2007a), the proportion of the observations identified as altered ($\omega_i < 1$) is 23%. The resulting posterior distribution from this model formulation, which accounts for (a) uncertainty regarding the spatial dependence in the SRM field, (b) the classification of observations as altered or not, and (c) observation noise, was sampled using Markov chain Monte Carlo. The model formulation is described in detail by Short, Higdon & Kronberg (2007a). Compared with previous methods that averaged the neighboring unedited RM(l, b), and then iteratively remove ‘‘outliers’’ (e.g. Simard-Normandin & Kronberg 1980 and other papers since then), the more statistically formal method used here is free of ad hoc criteria, for example on the decision of when to delete an

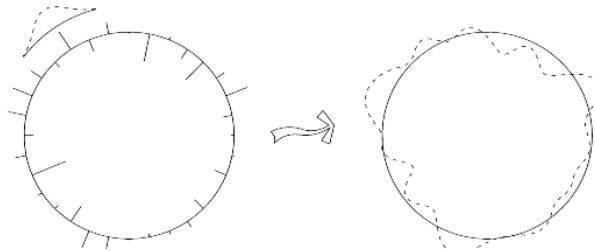


FIG. 1.— A realization of a process convolution model on the unit circle. The left panel shows knot locations and values (positive and negative), along with a smoothing kernel. The right panel shows the resulting Gaussian process realization obtained by a convolution of the knot values with the smoothing kernel.

outlier. Another important advance is that our model is with the data to produce the best estimate of the kernel width, rather than having it estimated, or guessed a priori.

Because this paper focuses on links between source redshift and RRM, it is important to search for possible bias effects of Galactic sky location on the z -distribution of the sources. As expected, the Galactic (l, b) locations of the RRM’s do not correlate with source redshift. Similarly, neither the amount of foreground RM correction, SRM, nor the uncertainty in the SRM show any trend with source redshift, after we isolated the optimum (l, b) zones as described below.

3. OPTIMIZATION OF THE DATASET AND INSPECTION OF BIAS EFFECTS

To ensure that other biases have not been introduced in the data selection we address three important issues that could potentially affect our statistical analysis. First, although the subtraction of the Galactic foreground is optimized, the quality of the SRM subtraction removal is (l, b) dependent, being generally less accurate at the lower Galactic latitudes. This leads to Galactic zone–based admission criteria for our sample, elaborated in section 3.1.

Secondly, our sample of radio sources is, typically, flux limited so that higher redshift objects tend to have higher luminosities. Thus we also investigate the $\text{RRM} - L_{\text{radio}}$ correlation to test for possible luminosity selection effects that could prejudice our search for a RRM - redshift relation.

Thirdly, errors in the individual RM measurements (separate from the Galactic foreground correction uncertainty) could conceivably exhibit a systematic redshift dependence, e.g. if the polarized signals were much weaker at larger redshifts. On investigation we find no significant correlation with redshift of the uncertainty of the individual RM determinations.

3.1. Optimal isolation of true extragalactic RM’s

To further minimize the uncertainties due to the subtraction of the Galactic component, SRM, we examined how the form of the overall RRM distribution varies as a function of the (l, b) region on the sky. We find that the width of the distribution $N(\text{RRM})$ for the smallest RRM’s decreases steadily as we raise the lower limiting latitude from $|b|=10^\circ$ (lower boundary) up to $|b| \approx 60^\circ$, but thereafter asymptotes to a stable value. In two dimensions, we find that the boundary can be lowered at some longitude zones without increasing the Galactic dispersion. An optimal subsample of 268 objects for which the influence

of SRM is minimized was thus obtained by accepting all sources at $|b| \geq 60^\circ$ as above, plus those having $b > 45^\circ$ and $l = 150 - 360^\circ$, and those with $b < -50^\circ$ at $l = 120 - 180^\circ$.

3.2. Checks for luminosity and other unwanted systematic effects on $\text{RRM}(z)$

Given that the radio luminosities of the sample span about six orders of magnitude, we can test whether the changing mean radio luminosity with redshift is likely to be significant. For the 268 radio source sub-sample we compared the rest-frame (“ k -corrected”) 2.7 GHz radio luminosity, $L_{2.7}$, with the *maximum* rest-frame RRM_{intr} . The latter assumes that *all* the RRM comes from magnetized plasma in the vicinity of the source, that is we multiply the observed RRM by $(1 + z_s)^2$ (eq. [1]).

At $z \lesssim 0.2$, where neither cosmological evolution nor intersection of the line of sight with an interloper are likely, the radio luminosities cover more than five orders of magnitude (Figure 2). However, we find no evidence for any correlation between $|\text{RRM}_{\text{intr}}|$ and $L_{2.7}$ (see Figure 2). To quantify this statement we parameterize the distribution in RRM_{intr} using a Lorentzian function

$$f(\text{RRM}; \Gamma/2) = \frac{1}{\pi} \frac{\Gamma/2}{(\Gamma/2)^2 + \text{RRM}^2}, \quad (3)$$

where $\Gamma/2$ is the width at half maximum, and we test for a $\Gamma/2 - L_{2.7}$ relation with

$$\Gamma/2 = w_0 (L_{2.7}/10^{21} \text{WHZ}^{-1})^\gamma. \quad (4)$$

The best fit parameters for this relation at $z < 0.2$ are: $w_0 = 36_{-24}^{+57} \text{rad/m}^2$ and $\gamma = -0.11_{-0.10}^{+0.12}$, confirming that there is no effect of $L_{2.7}$ on $|\text{RRM}_{\text{intr}}|$. The right hand panel of Figure 2 shows this graphically. Sources with lines of sight used to test for a correlation are represented as black dots. The blue stars and red squares are for lines of sight from sources at higher redshift. Due to the $(1+z_s)^2$ transformation they produce much larger $|\text{RRM}|$ values.

In conclusion, our test confirms the lack of any obvious $L_{2.7} - \text{RRM}$ relation. Note, however, that we cannot exclude the possibility that the highest redshift and most luminous sources could be affected by strong evolutionary effects due to the presence of enhanced magnetic fields when compared to their low redshift/low luminosity counterparts.

4. ANALYSIS OF THE RRM-REDSHIFT BEHAVIOR

Because of the statistical nature of the RM measurements and the present limited availability of supplementary optical data on individual lines of sight, the most

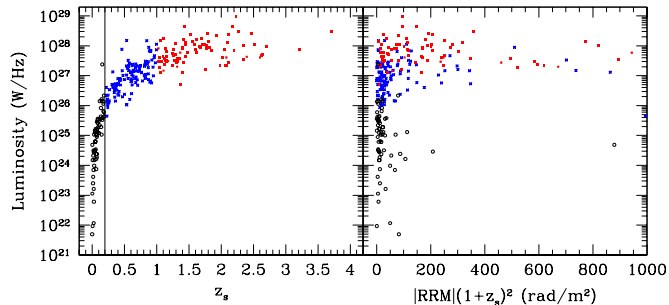


FIG. 2.— Left panel: Radio power at 2.7 GHz against redshift for the sample used in our analysis. The solid line marks the subsample ($z < 0.2$) used to test for a correlation between luminosity and intrinsic RRM. Right panel: Luminosity against RRM values transformed to the radio source rest frame (multiplied with $(1 + z_s)^2$). The empty circles are for the subsample at $z < 0.2$ that was used to test for a correlation between luminosity and RRM, the stars are those with $0.2 \leq z < 1.0$ and the solid squares are in the range $1.0 \leq z < 3.7$.

powerful diagnostic that we have is the *form* of the observed distribution $N(\text{RRM}, z)$, as a function of redshift.

To illustrate for the case of a source-intrinsic RM, if this were z -independent the observed RRM should monotonically decrease with increasing source redshift, due to the strong $(1 + z)^{-2}$ term (eq.(1)). This means that any variations in $N(\text{RRM}, z)$ at large z will arise from a competition between genuine evolutionary effects and the $(1 + z)^{-2}$ reduction. Thus, an interplay of different effects at $z \gtrsim 1$ might be expected.

On the other hand, in the case of intervening systems at low redshift their contributions to $|\text{RRM}|$ will be statistically invisible until there is a significant probability of intersecting an intervenor, at which point they will rise. Then at some sufficiently large z , the effect of incremental RM intersection depth may be overwhelmed by the $(1 + z)^{-2}$ term, which would tend to flatten any increase in the observed RRM. It may subsequently increase again if a sufficiently strong evolutionary increase sets in again at still larger redshifts. These possibilities set the context for our analyses in Section 5.

In the following we use a non-parametric approach, counting fractions of lines of sight f_i below a varying threshold RRM_i as a function of z (see Welter et. al 1984). We then apply a Kolmogorov-Smirnov test to examine the statistical significance of the redshift dependence in our data.

4.1. Evidence for Redshift Evolution

Figure 3 shows the observed distributions of RRM for 9 different redshift bins, each containing about 29 sources. At redshifts below $z \sim 1$ the distributions are characterized by a sharply defined mode at $\text{RRM} \approx 0$ plus a broader RRM component. Beyond this redshift, and especially at $z > 2$, the low-RRM component tends to get redistributed to larger RRM values.

This effect is shown quantitatively in Figure 4, where the fractions of lines of sight f_i below a varying threshold RRM_i are plotted as a function of redshift. The quantity f_{20} , representing the fraction of $|\text{RRM}|$'s below 20 rad m^{-2} , decreases significantly with redshift, from 72 % in the lowest two redshift bins ($\bar{z} = 0.08$) to 39% in the highest redshift bin ($\bar{z} = 2.34$). Similar, but progressively weaker trends occur for f_{40} and f_{100} respectively. The highest redshift bin shows the smallest value of f_i for all three thresholds. These trends indicate a clear evolution-

ary pattern which is most apparent at $|\text{RRM}| \lesssim 40 \text{ rad m}^{-2}$ in the *observer's* frame.

We confirm the reality of this redshift dependence with a Kolmogorov-Smirnov test. The entire sample was divided into two, below and above z_b and we compare the two normalized cumulative distributions of the absolute value of the RRM, $N(|\text{RRM}|)$ in Figure 5 (left panel). For $z_b \sim 1.8$, the samples are different at the 99% significance level. The RRM at which the maximum perturbation in the $N(|\text{RRM}|)$ occurs is typically between 10-25 rad m^{-2} (Figure 5, right panel). This shows that the clearest evolutionary signal comes from a broadening of the low- $|\text{RRM}|$ peak, rather than from outliers in the high RRM tails of the distribution.

The “migration” of some sources near $|\text{RRM}| = 0$ to wider wings works *oppositely* to the expected $(1 + z)^{-2}$ decrease. It clearly demonstrates that there is a global evolutionary effect in Faraday rotation. More precisely, as z increases up to and beyond ~ 2 , there is a gradual broadening of the distribution of RM's and a corresponding “depopulation” of the lowest $|\text{RRM}|$ bins, especially those $\leq |20| \text{ rad m}^{-2}$. In effect, at higher redshifts the Universe becomes progressively “Faraday opaque” as fewer sight-lines are able to “escape” an enhanced Faraday rotation at the higher z 's. The extra Faraday rotation is produced at $z > 1$ and is consequently greater in the Faraday rotating rest frame than what we observe, by a factor of $(1 + z)^2$. For example, $|\text{RRM}|$'s of 20 to 100 in Fig. 3 become 80 to 400 rad m^{-2} at $z = 1$ and 360 to 1200 rad m^{-2} if the Faraday rotation originates at $z = 2.5$.

Another striking illustration of this redshift effect is shown in Figure 6, which compares the normalized cumulative counts $N(< |\text{RRM}|)$ vs. $|\text{RRM}|$ above and below $z_b = 1$. Evolution in the high- $|\text{RRM}|$ tails remains to be better specified in future, larger samples at the highest redshifts, and we do not attempt to quantify it here. What is clear is that a significant evolution in the observed $|\text{RRM}|$ at modest RRM's begins to set in beyond $z \sim 1.0$.

5. QUANTITATIVE MODELLING TO ESTIMATE MAGNETIC STRENGTHS IN HIGH REDSHIFT SYSTEMS

In the following two subsections we take different approaches to the analysis and interpretation of the data. Each draws from the analysis framework developed in Welter et al. (1984).

First, in Section 5.1, we relate these results to recent

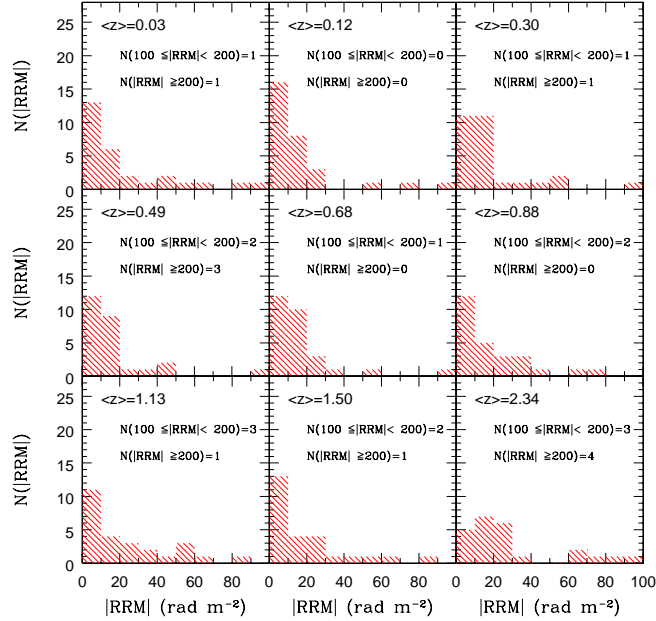


FIG. 3.— $|\text{RRM}|$ histograms of 268 lines of sight for different redshift bins having approximately equal numbers of lines of sight per bin. Redshift increases from the upper left to the lower right panel. The distribution in the highest redshift bin ($z \gtrsim 1.8$) is characterized by a significantly decreased “peak” near $|\text{RRM}| = 0$, and a corresponding significant broadening of the “low- $|\text{RRM}|$ ” peak to higher $|\text{RRM}|$ ’s.

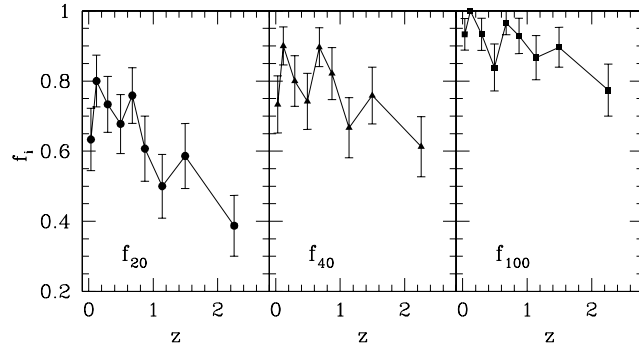


FIG. 4.— Fraction of lines of sight f_i below a threshold $|\text{RRM}_i$ as a function of redshift. Circles, triangles and squares show f_{20} , f_{40} and f_{100} respectively. Errors are calculated by randomly drawing lines of sight and calculating the r.m.s. of the resulting f_i distributions.

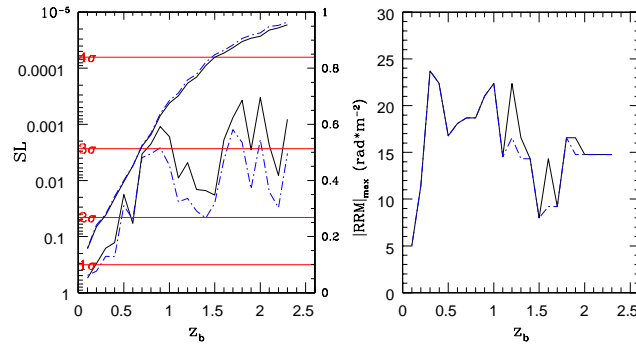


FIG. 5.— Left panel: Significance level (SL) of the KS test that the distributions of the RRM’s below and above z_b are not drawn from the same parent distribution. The black solid line is with no $|\text{RRM}|$ cut and the blue line is for lines of sight with $|\text{RRM}| < 200 \text{ rad/m}^2$. The dashed dotted lines give the fraction of lines of sight which are below z_b (right-hand axis). Right panel: The RRM value at which the normalized cumulative distributions, $N(\text{RRM})$ from the KS-test most differ, as a function of z_b .

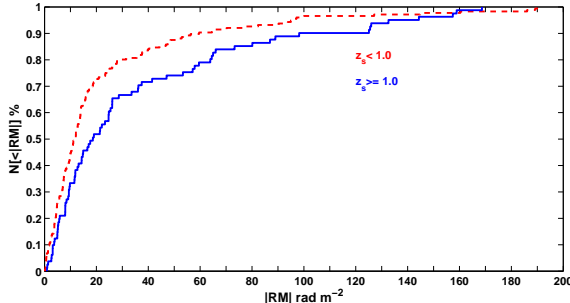


FIG. 6.— A comparison of the normalized cumulative counts of $N(<|\text{RRM}|)$ vs. $|\text{RRM}|$ shown separately for sources having $z < 1$ (upper curve) and $z > 1$ (lower curve). The clear separation between these two curves shows that excess RRM's introduced in the higher redshift subset are typically in the range $|\text{RRM}| \sim 20$ to $\sim 80 \text{ rad m}^{-2}$ in the observer's frame.

TABLE 1
PARAMETER VALUES FOR DIFFERENT RRM MODELS.

model	σ_{noise} (rad/m ²)	$\Gamma_{intr}/2$ (rad/m ²)	σ_{cloud} (rad/m ²)
no intervening systems	13^{+4}_{-3}	21^{+7}_{-6}	-
MgII systems with $W_r > 0.02\text{\AA}$	8^{+4}_{-2}	7^{+6}_{-4}	60^{+20}_{-15}
MgII systems with $W_r > 0.3\text{\AA}$	9^{+4}_{-2}	7^{+6}_{-4}	115^{+45}_{-30}

quasar optical absorption line data, given earlier evidence for an RM-absorption line association (e.g. Kronberg & Perry 1982, Welter et al. 1984, Oren & Wolfe 1995) and the *a priori* expectation that high column density absorption line systems will have an effect on RRM. We make model predictions of the $N(\text{RRM}, z)$ behavior based on previous MgII absorption line studies of quasars up to $z \sim 2.3$. In order to keep the number of free model parameters appropriate to the current state of the RRM data we assume no local cosmological evolution in the RRM intervenor systems, and we also exclude the very high RRM outliers from the analysis. We will show that, even in the absence of z -evolution and other contributions, MgII intervenor systems can have a recognizable influence on the observed RRM behavior described in §4.

In Section 5.2, we interpret the broadening in the distribution of $N(\text{RRM})$ at $z \gtrsim 1.5$ to draw general conclusions about the strength of early universe magnetic fields in galaxy systems up to $z \sim 3.5$.

5.1. RRM Intervenor model based on MgII absorber statistics

In this section we explore the possibility that MgII absorption systems are magnetized: Given their redshift distribution from QSO absorption line studies we investigate whether they can explain the observed statistical properties of the RM data and if so, what the implications are for their magnetic properties. Due to the poor statistics in the high-RM-tail of the distribution here we consider only lines of sight with an observed RRM value smaller than $|200| \text{ rad m}^{-2}$. Following Welter et al. (1984) we calculate the probability distribution function $P(\text{RRM}, z_s)$ for an observed RRM value of a source located at redshift z_s , as

$$P(\text{RRM}, z_s) = \sum_{n=0}^{n_{\max}} q_n(z_s) P_n(\text{RRM}, z_s). \quad (5)$$

Here P_n is the normalized probability distribution function of RRM for a line of sight to a source at redshift z_s passing through n intervenors. In addition, $q_n(z_s)$ is the probability of having n such intervenors along the line of sight which is given by Poisson's statistics:

$$q_n(z_s) = (n!)^{-1} \nu_s^n e^{-\nu_s}, \quad (6)$$

with

$$\nu_s = \int_0^{z_s} \frac{dN}{dz} dz \quad (7)$$

the mean number of intervening system out to z_s calculated using the MgII absorber distribution, dN/dz , described below. In addition to the effects of intervenors we also allow for contributions to the observed RRM from an intrinsic component and measurement errors, the latter dominated by uncertainties in the removal of the Galactic contribution. As a result, $P_n(\text{RRM}, z_s)$ is given by the convolution of the probability distribution functions associated with each individual component, namely

$$P_n(\text{RRM}, z_s) = P_{noise} * P_{n,interv}(z_s) * P_{intr}(z_s), \quad (8)$$

where for both the intervenor and intrinsic component we have explicitly indicated the redshift dependence.

In order to model $P_{n,interv}(\text{RRM}, z_s)$ we assume that each intervenor can be described as a cloud characterized by a number density of free electrons n_e , a size L and a randomly oriented magnetic field B with a coherence length l_C . Then for each intervenor we can define a probability distribution function, $P_{cloud}(\text{RRM}, z)$, given by a Gaussian distribution with $\sigma(z) = \sigma_{cloud}(1+z)^{-2}$, where

$\sigma_{cloud} \propto n_e B l_C (L/l_C)^{1/2}$, i.e. has units of RM. The contribution from n intervening systems is then given by the expression

$$AC_n \left[\int_0^{z_s} P_{cloud}(RRM, z) \frac{dN}{dz}(z) \right], \quad (9)$$

which is the convolution ($\mathcal{C}_n[\cdot]$) of n identical clouds distributed up to redshift z_s according to dN/dz , and A is a normalization factor. Note that expression 9 is valid even if $l_C \sim L$, provided that the magnetic field is randomly oriented from cloud to cloud and that the analysis is applied to a large number of RRM's associated with different lines of sight.

As for the intrinsic component, typically characterized by a non-Gaussian tail, we find it appropriate to use a Lorentzian distribution (eq. 3) which takes better account of the outlying RM values. Assuming for simplicity no source evolution, the latter can be fully characterized by a constant rest frame half width at half maximum, $\Gamma_{intr}/2$, which translates into an observed $\Gamma(z) = \Gamma_{intr} (1+z)^{-2}$. Finally, P_{noise} , the combination of the observational error in RM and the uncertainty in the SRM can be represented by a Gaussian width, σ_{noise} , which is independent of redshift.

In the following we carry out two separate analyses, one restricted to strong absorbers, i.e. those with an equivalent width $W_r \geq 0.3 \text{ \AA}$, and a second including weak absorbers, i.e. those with an equivalent width $0.02 \text{ \AA} \leq W_r \leq 0.3 \text{ \AA}$. For simplicity all the absorbers are characterized by the same σ_{cloud} , independent of redshift and equivalent width (or underlying column density).

For the weak MgII absorbers we use the function dN/dz obtained by Churchill et al. (1999) who investigated HIRES/Keck spectra of 26 QSOs in the redshift range $0.4 \leq z \leq 1.4$. They obtained the result

$$\frac{dN_{weak}}{dz} = (0.8 \pm 0.4) (1+z)^{1.3 \pm 0.9}. \quad (10)$$

Similarly, for the strong MgII absorption systems we utilize the results of Nestor et al. (2005) who, for the range $0.4 \leq z \leq 2.3$, find

$$\frac{dN_{strong}}{dz} = 1.001 (1+z)^{0.226} \times \left[\exp\left(\frac{-0.3}{\alpha(1+z)^\beta}\right) - \exp\left(\frac{-6.0}{\alpha(1+z)^\beta}\right) \right], \quad (11)$$

where $\alpha = 0.443$ and $\beta = 0.634$. Note that the different distributions of weak and strong intervenors, which enter the Poisson statistics (6) through the parameter ν_s defined in eq. (7), imply different values for the redshift at which an absorber is first encountered.

Using the probability distribution function in eq. 5, with the specific functional form detailed above, we now present the results of a maximum likelihood analysis which yields the parameters that best describe the data.

We begin by considering the influence of an RRM component due to strong MgII absorbers, in addition to an intrinsic component and Galactic foreground correction errors. The value of the parameters that produce the best fit to the data, in units rad m^{-2} , are

$$\begin{aligned} \sigma_{cloud} &= 115_{-30}^{+45}, \\ \Gamma_{intr}/2 &= 7_{-3}^{+6} \\ \text{and} \\ \sigma_{noise} &= 9_{-2}^{+4}. \end{aligned}$$

We note that, intriguingly, the typical derived value for σ_{cloud} is not very different from an RM observed for a typical line of sight through a (low z) spiral galaxy.

In order to illustrate how our model for $P(RRM, z_s)$ describes the data we define the quantile RRM_X via the relation

$$X = \int_{-RRM_X(z)}^{+RRM_X(z)} P(RRM, z) dRRM, \quad (12)$$

that is the value such that a fraction X of all the RRM's in a distribution P fulfills $|RRM| \leq RRM_X$. In Fig. 7 we plot both the observed data (points) and the model (solid-line) as a function of redshift for the quantiles $RRM_{0.68}$ (left) and $RRM_{0.90}$ (right).

It is apparent that our simple model with magnetized strong MgII absorbers is capable of reproducing the data distribution up to $z \sim 2$. The redshift dependence of the data in this model can be interpreted as follows. At low redshifts very few lines of sight pass through an intervenor so that $P(RRM, z_s)$ is dominated by the intrinsic and error components and varies only slowly with z . As z approaches ~ 1 , however, the probability of intersecting an absorbing system becomes significantly higher. Here the role of intervenors starts to kick in and $RRM_{0.68}$ grows gently. As we move to sources at progressively higher redshifts, the number of intervenors increases. However, their contribution is suppressed by the $(1+z)^{-2}$ dilution factor. This leads to a flattening in the distribution of $RRM_{0.68}$ at $z \sim 2$. Similar reasoning applies to $RRM_{0.90}$ except that the few intervenors encountered at low redshifts are able to affect this statistical quantity much earlier.

To illustrate the robustness of our estimate of σ_{cloud} , we show in Figure 8 contours of constant likelihood as a function of the parameters σ_{cloud} and $\Gamma_{intr}/2$ for two different choices of σ_{noise} , which will bracket a good fraction of the values this parameter can assume. It is apparent that a change in σ_{noise} affects $\Gamma_{intr}/2$, and that these two quantities are anticorrelated. This makes sense in that $\Gamma_{intr}/2$ and σ_{noise} dominate at low redshift where, to some extent, their role can be interchanged. Importantly, however, the uncertainties in the error estimate do not seem to have an impact on σ_{cloud} , which remains at about 3σ above the null value.

When we repeat the same analysis including the contribution of weak absorbers, the quality of the model prediction, represented by the dotted line in Fig. 5, worsens, particularly for the quantity $RRM_{0.68}$. This is because the number of intervenors encountered below redshift unity is substantially higher in the model, leading to a higher expected value for $RRM_{0.68}$. This result may indicate a limitation in our assumption of a column density independent σ_{cloud} for all absorbers. We expect that in attempting to reconcile the data with the model, improving on this limitation would provide a better solution than postulating drastically different magnetic properties for weak and strong MgII absorption systems. Also, establishing a $W_r = 0$ control sample, not available in this investigation, will improve future parameter specifications for MgII intervenors.

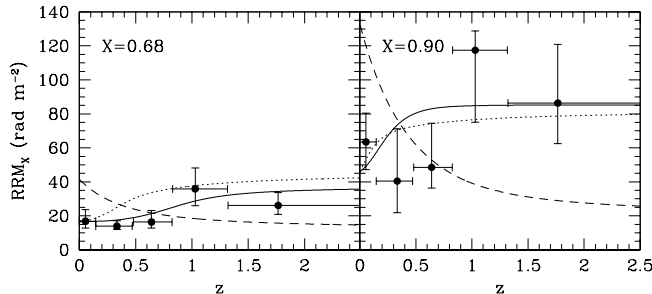


FIG. 7.— Quantiles $RRM_{0.68}$ (left panel) and $RRM_{0.90}$ (right panel) as a function of redshift are shown for the observed RRM data and different models. The solid lines show a model with strong ($W_r > 0.3\text{\AA}$) MgII absorbers. The dotted lines show a model where the weak ($0.02\text{\AA} < W_r \leq 0.3\text{\AA}$) absorbers are included for comparison. The dashed lines show a model incorporating SRM removal error and a non-evolving intrinsic contribution. Each bin contains about 51 lines of sight, and we show the median redshifts. Errors in the quantiles are calculated with the bootstrap method, with the 1σ confidence interval shown. The derived parameter values are summarized in Table 1.

Finally, we show a model in Figure 7 (dashed line) in which we set $\sigma_{cloud} = 0$, i.e., which has only an unchanging intrinsic component and a measurement error. The dashed lines in both panels of Fig.7 show the quantiles $RRM_{0.68}$ and $RRM_{0.90}$ predicted by this model, with best fit parameters, in units of rad m^{-2} , $\sigma_{noise} = 13_{-3}^{+4}$ and $\Gamma_{intr}/2 = 21_{-6}^{+7}$. It clearly fails to reproduce the behavior of the observed RRM statistics with redshift. The reason this model fails so dramatically is that, since the noise component is independent of redshift and the RM of the non-evolving intrinsic component declines as $(1+z)^{-2}$, it can only predict a decrease of both quantiles as a function of redshift, instead of the observed increase.

5.2. Implications for magnetic fields in early systems

Whether due to intervenors or other evolution of galactic or pre-galactic systems, the rise in the fraction of lines of sight affected by Faraday rotation at progressively higher redshifts indicates the presence of magnetized gas in such systems at earlier epochs. While the intervenor model would explain the behavior of the data with the higher incidence of magnetized clouds, an alternative possibility that we cannot yet exclude is that the RRM in the high redshift sources is dominated by an intrinsic component that increases into the past. Note that in this case, however, we require substantial *negative* evolution in the Faraday-active medium, i.e. with decreasing z , in order not to over-predict the expected dispersion in the observed RRM values at low redshift (see Figure 7). In terms of our model parameters, for example, Γ_{intr} would have to decrease with time. This would follow naturally if the Faraday active medium were a magnetized cloud expanding as a result of being over-pressured with respect to the ambient medium.

In any case we can attempt to estimate the strength of the magnetic field in these earlier systems, given some independent estimate of the column density of free electrons, N_e . Following Kronberg and Perry (1982), we can express an RRM_C arising at redshift z_C as

$$RRM_C = \beta(1+z_C)^{-2} N_e \langle B_{\parallel} \rangle \text{rad m}^{-2}, \quad (13)$$

where N_e is in cm^{-2} , $\langle B_{\parallel} \rangle$ accommodates any field reversal

pattern, and is defined by

$$\langle B_{\parallel} \rangle = \frac{\int_{cloud} n_e B_{\parallel} dl}{\int_{cloud} n_e dl}. \quad (14)$$

The constant $\beta = 2.63 \times 10^{-13} \text{ rad m}^{-2} \text{ cm}^2 \text{ Gauss}^{-1}$.

The rms deviation from zero of the observed RRM, σ_{RRM} , can be straightforwardly converted to an estimate of a typical $\langle B_{\parallel} \rangle$ by inverting Eq. (13) and inserting an estimate of N_e for the system generating the Faraday rotation. The important point is that as we move into the redshift range $1.8 \lesssim z \lesssim 3.7$ the fraction of lines of sight, f_i , with near zero RRM, falls off sharply. This is independent of whether the excess RRM is in the vicinity of the radio source (“intrinsic”), or located in a galaxy system at intervening redshift. Note that the exact redshift is not crucial for our estimate here as the spread in $(1+z)^2$ over the interval $1.8 \lesssim z \lesssim 3.7$ is modest, of order a few at most.

Inverting Eq. (13) and setting $RRM_C \sim \sigma_{RRM}$ in the observer’s frame (e.g. panel 9 of Fig.3) gives

$$\langle B_{\parallel} \rangle = 5.5 \times 10^{-7} \text{G} \left(\frac{1+z_C}{3.5} \right)^2 \times \left(\frac{\sigma_{RRM}}{20 \text{ rad m}^{-2}} \right) \left(\frac{N_e}{1.7 \times 10^{21} \text{cm}^{-2}} \right)^{-1} \quad (15)$$

for the system causing the RRM excess.

The local $\langle B_{\parallel} \rangle$ values within a system are expected to be larger because of cancellations due to reversals in the magnetic field orientation along the line of sight. The column density assumed in the above normalization is comparable to HII column densities through today’s typical spiral galaxies. Thus if the RRM is due to galactic systems at high redshifts, our estimate would imply the presence of magnetic fields there with strength of order at least a μG , which is comparable to the value observed in the Galaxy. If the radio source is embedded *within* a Faraday rotating cloud (the intrinsic RRM case), the $\sim 2 \times$ lower RRM pathlength would, relative to a lower z intervening cloud, make the magnetic field strength correspondingly higher. The results presented in §4.1 indicate that magnetic fields must have been generated very quickly in galaxy systems, at early cosmological epochs.

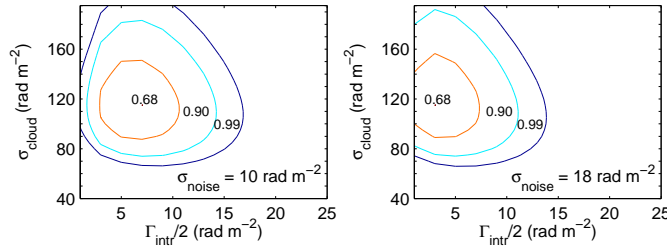


FIG. 8.— Contours of constant likelihood as a function of fit parameters $\Gamma/2_{intr}$ and σ_{cloud} for two fixed values of σ_{noise} . MgII systems with $W_r > 0.3\text{\AA}$ are used as a model for the intervening systems.

6. ON THE DETECTABILITY OF A WIDESPREAD IGM MAGNETIC FIELD

Limits on a widespread IGM magnetic field were first discussed and derived in the 1970's under the assumption that the Universe was homogeneous, had only baryonic matter, and was pervaded by contiguous magnetized cells of comoving length, l_0 . Under these assumptions, RM's measured at the largest redshifts (then ~ 2) placed upper limit estimates of B_0^{IGM} in the range 10^{-8} - 10^{-9} G (Rees & Reinhardt (1972), Nelson (1973), Kronberg & Simard-Normandin (1976), Kronberg et al. (1977)). In this co-expanding model in which $|B(z)| \propto (1+z)^2$, the observed growth in $\text{RRM}(z)$ due to a widespread, co-expanding IGM is dominated by contributions at the largest redshifts. In the context of current concordance cosmology, and our knowledge of large scale filaments and voids of matter, these B_0^{IGM} limits are no longer appropriate, and need to be revisited.

Now, isolating or limiting a widespread extragalactic RRM, and hence B_0^{IGM} , is more difficult. It requires that we disentangle a B^{IGM} from any cosmic evolution in $\text{RRM}_C(z)$ (case 2) and RRM_{intr} (case 3). At least some of the high redshift sources in our sample, such as 3C191 at $z=1.95$ (Kronberg et al. 1990), and several high- z RM's measured by Carilli et al.(1997), Athreya et al. (1998), and Pentericci et al. (2000) indicate evolutionary effects in RRM_{intr} .

However the expected width of $N(\text{RRM}_{\text{IGM}}, z)$ due to a widespread, co-expanding magnetized IGM increases steeply at the large redshifts (e.g. Kronberg, Reinhardt & Simard-Normandin 1977). This raises the possibility that future RRM datasets that extend to redshifts $z = 4 - 5$ may be strongly influenced by a widespread co-expanding intergalactic medium.

Then with better knowledge of the intervenor and source-intrinsic populations, $\text{RRM}_C(z)$ and $\text{RRM}_{intr}(z)$, it may be possible to explore, or limit the contribution of $\text{RRM}_{\text{IGM}}(z)$. The data could then be compared with modelled contributions of $\text{RRM}_{\text{IGM}}(z)$ (filaments) and $\text{RRM}_{\text{IGM}}(z)$ (voids) based on LSS evolution simulations.

A probe of the RRM contribution of some local universe galaxy filaments was recently attempted by Xu et al. (2006). Their initial estimate was $B_{\text{IGM}} \sim 3 \times 10^{-7}\text{G}$ in the Perseus-Pisces supercluster filament zones, scaled to an assumed field reversal scale of ~ 0.5 Mpc and to estimates of the electron density in the warm-hot IGM(WHIM).

7. SUMMARY AND CONCLUSIONS

We have analyzed an unprecedented large sample of RRM data extending to redshift 3.7. The size of our new Faraday RM sample permits us to isolate preferred Galactic (l, b) zones where Galactic foreground RM is optimally removed with the help of a new, more accurate set of 1566 extragalactic source RM's that are mostly off the Galactic plane. We find a clear increase with redshift of Galaxy-corrected RRM's at medium to low RRM levels, below $\sim 100 \text{ rad m}^{-2}$ in the observer's frame. Our results and conclusions can be summarized as follows:

1. There is a striking and systematic decline, significant at the $\sim 3 \sigma$ level, in the fraction of sources in the range $z \sim 1.5 - 2.3$ that have $|\text{RRM}|$ less than 20 rad m^{-2} . This is the first global indication that the Universe becomes increasingly "Faraday opaque" to the highest redshift radio sources.
2. A model with intervening systems distributed according to the dN/dz statistics of strong MgII absorption line systems in QSO spectra is consistent with the observed growth in the widths of the RRM distribution up to $z \sim 2$ with no evolution in the rest frame RM of each absorber. This hypothesis could be tested in the future by comparing the distribution of RM in quasar sightlines that have, and do not have, strong MgII absorption.
3. We provide global estimates of early Universe magnetic field strengths in galaxy systems, based on the progressively increasing "Faraday opaqueness" of systems beyond $z \sim 1.5$. These have at least μG level fields, and indicate that magnetic fields at these high redshifts were at least as strong as at the present epoch.
4. Redshift variations in the widths of RRM distributions below $z \sim 1.2$ are small and can only be specified at the $1.5 - 2\sigma$ level, limited by residual uncertainties in the foreground Galactic RM. The latter is at the level of $\sim 9 \text{ rad m}^{-2}$ in the higher b zones selected, determined from a new all-sky sample of 1566 RM's.

8. ACKNOWLEDGEMENTS

We thank Chris Carilli and Meri Stanley of NRAO for access to VLA data that enabled us to calculate several additional high - z RM's, and an anonymous referee for helpful comments. PPK acknowledges support from the

U.S. Department of Energy, the Laboratory Directed Research and Development Program (LDRD) at Los Alamos National Laboratory, and the Natural Sciences and Engineering Research Council of Canada (NSERC). MLB is

supported by the Swiss National Science Foundation, and FM acknowledges support by the Swiss Federal Institute of Technology through a Zwicky Prize Fellowship.

REFERENCES

- Armengaud, E., Sigl, G., and Miniati, F. 2005 PRD **72**, 43009
 Athreya, R. M., Kapahi, V. K., McCarthy, P. J., & van Breugel, W. 1998, A&A, 329, 809 - 820
 Carilli, C. L., Perley, R. A., Dreher, J. W., & Leahy, J. P. 1991, ApJ, 383, 554
 Carilli, C. L., Roettgering, H. J. A., van Ojik, R., Miley, G. K., & van Breugel, W.J.M. 1997, ApJS, 109, 1
 Churchill, C. W., Rigby, J. R., Charlton, J. C., & Vogt, S. S. 1999, ApJS, 120, 51
 Dolag, K., Grasso, D., Springel, V. and Tkachev, I. JCAP 01(2005) 009;
 Kolatt, T. 1998, ApJ, 495, 564-579
 Kronberg, P. P., & Perry, J. J. 1982, ApJ, 263, 518-532 L31-L34
 Kronberg, P. P., Perry, J. J., & Zukowski, E. L. H. 1990, ApJ, 355, L31-L34
 Kronberg, P. P., Perry, J. J., & Zukowski, E. L. H. 1992, ApJ387, 528-535
 Kronberg, P. P. & Simard-Normandin, M. 1976 *Nature* 263, 653 - 656
 Kronberg, P. P., Reinhardt, M., & Simard-Normandin, M. 1977, A&A, 61, 771
 Kronberg, P. P., Dufton, Q. W., Li, H., & Colgate, S. A. 2001, ApJ, 560, 178
 Mestel, L., & Paris, R. B. 1984, A&A, 136, 98
 Nelson, A.H. 1973, *Pub. Astron. Soc. Japan*, 25, 489
 Nestor, D. B., Turnshek, D. A., & Rao, S. M. 2005, ApJ, 628, 637
 Oren, A. L., & Wolfe, A. M. 1995, ApJ, 445, 624
 Pentericci, L., Van Reeve, W., Carilli, C. L., Röttgering, H. J. A., & Miley, G. K. 2000, A&AS, 145, 121
 Rees, M. J. 1987, QJRS, 28, 197
 Rees, M. J. & Reinhardt, M. 1972, A&A19, 104,
 Sigl, G., Miniati, F., and Ensslin, T. A. 2003 PRD 68, 043002
 Sigl, G., Miniati, F., and Ensslin, T. A. 2004 PRD 70, 043007
 Short, M. B., Higdon, D. M., & Kronberg, P. P. 2007a *Bayesian Analysis* (in press) <http://ba.stat.cmu.edu/forthcoming.php>
 Short, M. B., Higdon, D. M., & Kronberg, P. P. 2007b *Bayesian Statistics* **8**, 665 - 660
 Welter, G. L., Perry, J. J. & Kronberg, P. P. 1984, ApJ, 279, 19-39
 Xu, Y., Kronberg, P. P., Habib, S., & Dufton, Q. W. 2006 ApJ, 637, 19
 You, X. P., Han, J. L. & Chen, Y. 2003 *Acta Astronomica Sinica*, 44, 155